Preprints of the 21st IFAC World Congress (Virtual)
Berlin, Germany, July 12-17, 2020

Acoustic Radiation Force Impulse Imaging Using Displacements of Lateral Dimension

Shengnan Zhang, Yanbin Xu, Xuyang Bao, Feng Dong

Tianjin Key Laboratory of Process Measurement and Control,
School of Electrical and Information Engineering, Tianjin University,
Tianjin 300072 China (e-mail: xuyanbin@tju.edu.cn)

Abstract: Acoustic radiation force (ARF) induced elasticity imaging is usually used to obtain the elastic properties of media by detecting the induced displacement at the focal point. However, the ARF induced displacement response actually appears not only at the focal point, but also in lateral dimension at the focal depth. The relationship between the stiffness of media and the axial-directional displacements in lateral dimension at the focal depth has been analyzed through theoretical derivation, simulation and experimental verification. The results demonstrate that the maximum displacement in lateral dimension is inversely proportional to the lateral distance from the currently estimated point to the focal point. Therefore, the maximum displacement in lateral dimension at the focal depth is capable of estimating the elastic properties of the media. Based on this conclusion, an ARF impulse imaging method using displacements of lateral dimension is proposed. The induced displacements at the focal point as well as in the lateral dimension at the focal depth are detected under only the focal point excited. In this way, the proposed imaging method is expected to broaden the ARF impulse imaging region from the focal point to a larger region in the lateral dimension while reducing patient acoustic exposure and transducer heating.

Keywords: ultrasound elastography, acoustic radiation force impulse, displacement analysis, lateral dimension, imaging region

1. INTRODUCTION

Elastic properties are important diagnostic indicators related to physiological and pathological condition, which are the intrinsic mechanical properties of soft tissues. Several groups have been exploring the feasibility of ultrasound elastography methods for imaging tissue structure (Dietrich *et al.* 2017, Doyley *et al.* 2014). During the propagation of ultrasound, acoustic radiation force (ARF) is generated due to the transfer of wave momentum (Westervelt *et al.* 1951, Torr *et al.* 1984). Recently, the ultrasound elastography methods based on ARF excitation that produce an ARF to generate localized displacement responses and shear wave propagation in the measured field have been investigated (Doherty *et al.* 2013).

In 2001, the acoustic radiation force impulse (ARFI) imaging method has been developed by Nightingale to image local variations in mechanical characteristics of soft tissues (Nightingale *et al.* 2001). A single focused ultrasound transducer is applied to both induce and measure the displacement responses in the focal region. The results have demonstrated that the displacement responses are inversely proportional to the stiffness of soft tissues, which causes high contrast in variation of tissue stiffness. In 1998, the shear wave elasticity imaging (SWEI) method has been proposed by Sarvazyan to characterize and image soft tissue structures (Sarvazyan *et al.* 1998). A single focused ultrasound transducer is used to produce a sufficient ARF in the focal region to cause shear waves propagation, which are monitored at multiple lateral directions divided by a known distance from the focal region. The propagation velocity of shear wave can be calculated by the time information of displacements at these different lateral positions. Then the distribution of elastic characteristics in the measured field can be reconstructed by the velocity of shear wave. In 2015, in order to extend the axial region of excitation, a rapid multi-focal zone ARFI imaging method has been investigated by Nightingale (Rosenzweig *et al.* 2015). The contrast to noise ratio can be improved, while the image quality is reduced slightly. In 2017, Zhou proposed a multi-functional ultrasonic micro-elastography imaging method, in which ARFI imaging and SWEI are both implemented (Qian *et al.* 2017).

Traditional ARFI imaging method is usually used to obtain the elastic properties of media by detecting the induced displacement at the focal point. However, the ARF induced displacement response actually appears not only at the focal point, but also in lateral dimension at the focal depth. The objective of this proposed method is to make full use of information from the displacements in lateral dimension at the focal depth to estimate the elastic properties of media. The relationship between the stiffness of media and the axial-directional displacements in lateral dimension at the focal depth is established through theoretical derivation, simulation and experimental verification.

The analysis results demonstrate that the maximum displacement in lateral dimension is inversely proportional to the lateral distance from the currently estimated point to the focal point, and further prove that the maximum

displacement in lateral dimension at the focal depth is capable of evaluating the elastic properties of the media.

Based on this conclusion, a novel ARFI imaging method which not only detects the induced displacement at the focal point but also utilizes displacements in lateral dimension at the focal depth is proposed. The elastic properties can be reflected by the maximum displacements in lateral dimension at the focal depth directly. The simulation and experimental results have validated that the elastic distribution of the measured field can be reconstructed by the maximum displacements in lateral dimension.

In this way, the proposed imaging method is expected to broaden the ARF impulse imaging region from the focal point to a larger region in lateral dimension while reducing patient acoustic exposure and transducer heating.

2. METHOD

2.1 Acoustic Radiation Force

ARF generation attributes to the transfer of wave momentum when ultrasonic wave is propagating in soft tissues with absorption and scattering properties (Westervelt *et al.* 1951, Torr *et al.* 1984). ARF in the direction of ultrasonic wave propagation is (Nightingale *et al.* 2001)

$$F = (\Pi_a + \Pi_s - \int \gamma \cos\theta r dr d\theta)\langle E \rangle \tag{1}$$

where F is the generated ARF, Π_a and Π_s are the total power caused by absorbing and scattering, γ is the amplitude of scattered intensity, θ is the scattering angle of ultrasonic wave, $rdrd\theta$ is an area element, and $\langle E \rangle$ is the temporal average energy density of the ultrasonic wave.

Under the plane wave assumption, the ARF F generated in an absorbing soft tissue becomes

$$F = \frac{2\alpha I}{c} \tag{2}$$

where c is the velocity of ultrasonic wave, α is the absorption coefficient of soft tissues, and I is the temporal average intensity of ultrasonic wave.

2.2 Tissue Responses to Acoustic Radiation Force

In ultrasound elastography methods based on ARF excitation, a focused ultrasound transducer is used to generate sufficient ARF in the focal region to cause localized displacement responses and shear wave propagation, and the physical model is illustrated in Fig. 1. Assuming that the tissue is linear, elastic, and isotropic, the governing equation can be described as (Doyley *et al.* 2012)

$$\mu\nabla^2\mathbf{u} + (\lambda + \mu)\nabla(\nabla \cdot \mathbf{u}) + \mathbf{F} = \frac{\partial^2 \mathbf{u}}{\partial t^2} \tag{3}$$

where λ and μ are Lame constants related to Young's modulus E and Poisson's ratio v, $\mathbf{F}$ is the vector form of the ARF F, $\mathbf{u}$ is the generated displacement caused by external force and internal stress, and $\frac{\partial^2 \mathbf{u}}{\partial t^2}$ is the acceleration, ρ is the density of soft tissues.

Since the ARF applied to soft tissue is a pulsed form at the focal region, it can be expressed as (Li *et al.* 2017)

$$\mathbf{F} = \delta(\mathbf{x})\delta(t)\mathbf{f} \tag{4}$$

where $\mathbf{f}$ is a vector, which is parallel to the direction of ultrasonic wave propagation, and the impulse function $\delta(\mathbf{x})$ and $\delta(t)$ indicate that $\mathbf{f}$ is applied to the position $\mathbf{x}$ at time t. Combing (3) and (4), the equilibrium equation can be expressed as

$$\mu u + (\lambda + \mu)u + \delta(\mathbf{x})\delta(t)\mathbf{f} = \frac{\partial^2 u}{\partial t^2} \tag{5}$$

where u is the axial-directional maximum displacement of the element along the force direction. The initial conditions ($t = 0$) are

$$u = 0 \ \ and \ \ \frac{\partial u}{\partial t} = 0 \tag{6}$$

According to the initial conditions, (5) can be solved by Green function (Bercoff *et al.* 2004). Therefore, the maximum displacement at position $\mathbf{x}$ generated by ARF is

$$u \approx \frac{f}{4\pi\rho c_T^2} \cdot \frac{1}{x} \cdot \delta\left(t - \frac{x}{c_T}\right) \tag{7}$$

where f is the amplitude of $\mathbf{f}$, x is the distance from position $\mathbf{x}$ to the focal region, c_T is the shear wave velocity, which can be expressed by (Doherty *et al.* 2013)

$$c_T = \sqrt{\frac{\mu}{\rho}} \tag{8}$$

Assuming that the Poisson's ratio v of soft tissue is about 0.5, so the relationship between c_T and Young's modulus E is

$$E = 3\rho c_T^2 \tag{9}$$

Therefore, (7) can be transformed by

$$u \approx \frac{3f}{4\pi E} \cdot \frac{1}{x} \cdot \delta\left(t - \frac{x}{c_T}\right) \tag{10}$$

The impulse function $\delta(t - \frac{x}{c_T})$ means that the maximum displacement at position $\mathbf{x}$ is generated when the shear wave propagates to that position.

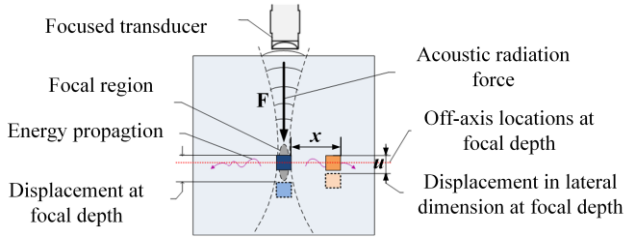

Fig. 1. Physical model of ultrasound elastography methods based on ARF excitation.

2.3 Displacement Analysis in Lateral Direction

The maximum displacement generated by shear wave propagation at each position is considered, regardless of the process of shear wave propagation. Therefore, the impulse function $\delta(t - \frac{x}{c_T})$ could be eliminated, and (10) can be expressed as

$$u \approx \frac{3f}{4\pi E} \cdot \frac{1}{x} \tag{11}$$

From (11), it can be seen that the maximum displacement is inversely proportional to the Young's modulus and the distance from focal region. In order to make full use of the maximum displacement information in the lateral dimension, the relationship of maximum displacement and the position at lateral direction is further studied.

Take the logarithm of both sides of (11), it becomes

$$\lg u = -\lg x + \lg m - \lg E \tag{12}$$

$$m = \frac{3f}{4\pi} \tag{13}$$

Therefore, in logarithmic scales, the maximum displacement decays linearly as the distance from focal region increases. If $\lg x$ is treated as an independent variable and $\lg u$ is treated as a dependent variable of $\lg x$, $\lg m - \lg E$ can be taken as Y-intercept of the linear function between $\lg u$ and $\lg x$. It can be seen that the value of Y-intercept is inversely related to the Young's modulus of soft tissue.

Equation (11) and (12) can reveal the relationship among maximum displacement, lateral distance and Young's modulus of soft tissues. According to these relationships, relationship curves between the maximum displacement and the lateral distance have been illustrated as Fig. 2(a) and (b), where $m = 1 \times 10^{-3}$ kg·m/s^2. According to (11), when Young's modulus E is large enough to a certain extent, the change of maximum displacement u due to the change of E becomes very small, so in that range it is difficult to distinguish media with different Young's modulus from Fig. 2(a), for example, when the Young's modulus is 50 kPa and 100 kPa respectively. According to (12), the Young's modulus on each curve have direct effects on the Y-intercepts. In Fig. 2(b), both of the coordinate axes are logarithmically processed, and it can be seen that the different lines have different Y-intercepts which are directly inversely related to the Young's modulus. That is, the medium with small Young's modulus may have great Y-intercept. Based on this conclusion, an ARF impulse imaging method using displacements of lateral dimension is proposed.

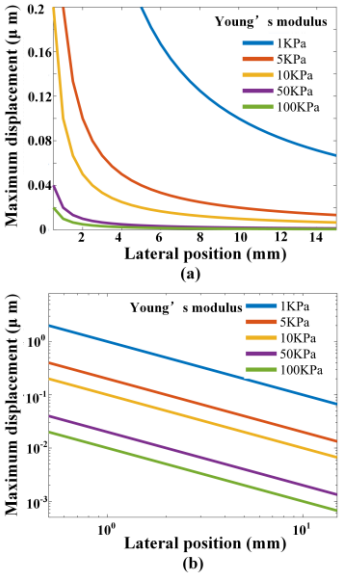

Fig. 2.Maximum displacements under different Young's modulus in lateral direction at the focal depth. (a) With linear scales. (b) With logarithmic scales.

3. SIMULATION AND DISPLACEMENT ANALYSIS

The maximum displacements are analysed at the focal region, and in the lateral direction at the focal depth. The feasibility of ARFI imaging method using displacements of lateral dimension has been explored by some phantoms with different inclusions through simulation.

3.1 Displacement Analysis

An inhomogeneous phantom simulation model with measured field $30\,\text{mm} \times 30\,\text{mm}$ was constructed by COMSOL Multiphysics® 4.4, as shown in Fig. 3. A stiff square inclusion with a side length of 4 mm was set at the

focal depth from the lateral direction 4 mm to 8 mm, which is marked by the dashed red lines. The Young's modulus of the background medium and the inclusion were set as 5 kPa and 50 kPa. The density and attenuation coefficient of media were 1.0 kg/m^3 and 0.7 dB/cm/MHz, and the focused transducer below the measured field was excited by signal with 3.5 MHz frequency and 0.1 ms duration time. The velocity of ultrasound was set as 1540 m/s. The maximum displacements were calculated by finite element method.

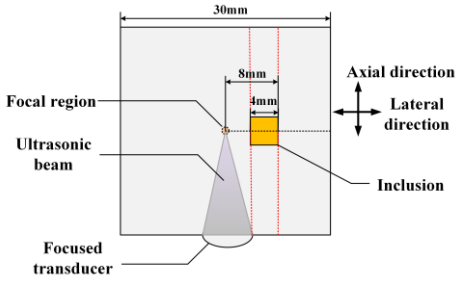

Fig. 3. Schematic diagram of simulation configurations.

Fig. 4 explores whether the maximum displacement in lateral direction at the focal depth is capable of reflecting the elastic distribution. Fig. 4(a) shows the computed maximum displacements in lateral direction with an inclusion at the focal depth. The blue curve in Fig. 4(b) shows the measured maximum displacements, and the dashed red line marks the true position of inclusion. All of the coordinate axes are logarithmically processed. From Fig. 4(b), the maximum displacements decline linearly at about 0-3 mm, 4 mm-8 mm, and 10 mm-18 mm in the lateral direction, which means that the Young's modulus of each segment is the same. While the maximum displacements drop rapidly at about 3 mm-4 mm, which indicates that there could be a big increase of Young's modulus. Moreover, the maximum displacements increase significantly at about 8 mm-10 mm, which represents that there could be a fall-off of Young's modulus. It can be seen that the position where the maximum displacements vary rapidly is consistent with the position of inclusion.

The results demonstrate that maximum displacements in lateral dimension at the focal depth can reflect the distribution of elastic properties through the displacement attenuation characteristics, and can be capable of determining the size and boundary of the inclusion effectively without too much complicated data processing.

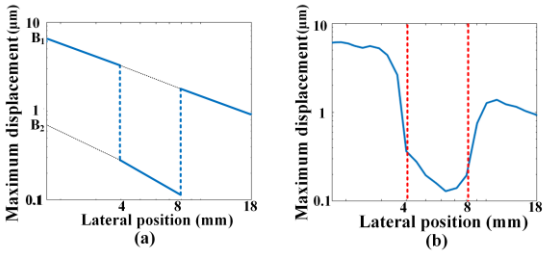

Fig. 4. Maximum displacements in lateral direction at the focal depth. (a) Computed maximum displacements. (b) Measured maximum displacements.

3.2 Reconstruction Results

In order to further investigate the feasibility of this proposed method, three phantoms (I), (II) and (III) with different inclusions were constructed, as shown in Fig. 5(a). Each phantom was composed of two media with different Young's modulus, where the grey area represents soft medium with Young's modulus of 5 kPa, and the black area is stiff medium with Young's modulus of 50 kPa. The region of ARF applied is marked as blue, and the measured field studied shown in Fig. 5(b) is marked with a red dotted line in Fig. 5(a). The maximum displacements in lateral direction at the focal length, which is marked with a red dotted line in Fig. 5(b) are analysed.

Fig. 5(c) and (d) display the maximum displacements in linear scales and logarithmic scales respectively, where the horizontal axes represent the distance from the focal region, and the vertical axes are the maximum displacement generated at the corresponding position. Fig. 5(c) shows that the maximum displacement declines rapidly as the distance from the focal region increases, so the difference in elastic properties cannot be distinguished by displacement directly. However, from Fig. 5(d), it can be seen that in logarithmic scales, the attenuation of maximum displacement is linear as the distance from the focal region increases for the same Young's modulus, while the maximum displacement will vary significantly if there is a change in Young's modulus. In logarithmic scales, for the linear function between the maximum displacements and the distance from focal region, all the slopes corresponding to media with different Young's modulus are the same, while the values of Y-intercept are inversely related to Young's modulus. Therefore, the inclusions could be identified by maximum displacements directly in logarithmic scales.

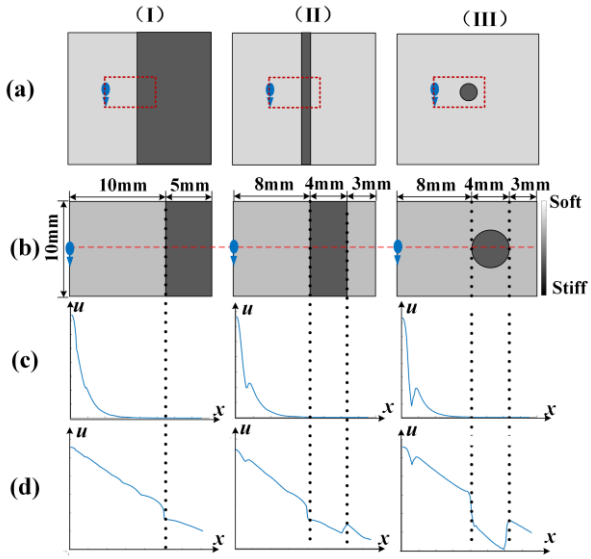

Fig. 5. Phantoms with different inclusions in simulation. (a). Simulation model (b) Measured field. (c) Maximum displacements at lateral direction in linear scales. (d) Maximum displacements at lateral direction in logarithmic scales.

The reconstructed results are illustrated in Fig. 6. The images reconstructed from maximum displacements in lateral dimension in linear scales and in logarithmic scales are shown in Fig. 6(b) and Fig. 6(c). Comparing these two columns, the distribution of elastic properties in media can be reconstructed in logarithmic scales but not in linear scales.

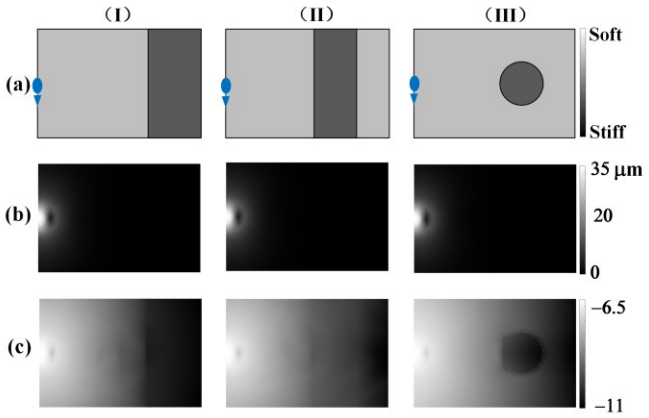

Fig. 6. Simulation results. (a) Measured field. (b) Images reconstructed in linear scales (c) Images reconstructed in logarithmic scales.

4. EXPERIMENTAL

The experimental system is illustrated in Fig. 7. Two single-element transducers were applied in this system. One of the transducers with central frequency of 3.5 MHz, which was called pushing transducer, was used to generate ARF to cause displacement responses. The other transducer called tracking transducer, which was placed on the opposite side of the pushing transducer, was used for acquiring RF echo data. A function generator (AFG3252, Tektronix, USA) was used along with an RF power amplifier (25A250, Amplifier Research, USA) to generate the excitation signal for pushing transducer. The excitation signal was a sinusoidal tone burst with a peak-to-peak amplitude of 80 V and a duration time of 0.1 ms. An ultrasonic pulser-receiver (5077PR, Olympus, USA) was used to excite the tracking transducer with a peak-to-peak amplitude of 100 V and a pulse repetition frequency of 5 kHz. A stepper motor was applied for mechanical scanning of the tracking transducer in the lateral direction, and the step size of each scan was 0.5 mm. These RF echo data acquired from tracking transducer were processed by phase-shift estimation method to calculate maximum displacement responses (Viola *et al.* 2003).

In Fig. 8(a), three phantoms were made of different concentrations of agar and the same concentration of graphite powder to simulate media with different distributions (Hall *et al.* 1997). The background and inclusion of all these phantoms were 25 kPa and 525 kPa respectively, which are marked with grey and black. The region of ARF applied is marked as blue, and the direction of ARF is indicated by an arrow. The measured field displayed in Fig. 8(b) is marked with a red dotted line in Fig. 8(a).

The images reconstructed in logarithmic scales are shown in Fig. 8(c). The experimental results demonstrate that this proposed method can distinguish media with different Young's modulus, and can reconstruct the measured field by maximum displacements in the lateral dimension at the focal depth directly. In this method, the pushing transducer is fixed, and does not require scanning the measured field. In addition, the maximum displacements in the lateral direction can reflect the elastic properties directly, rather than calculating the propagation velocity of shear wave by the time information of displacements at these different lateral locations. Therefore, the experimental system and process can be simplified, and the imaging region can be extended.

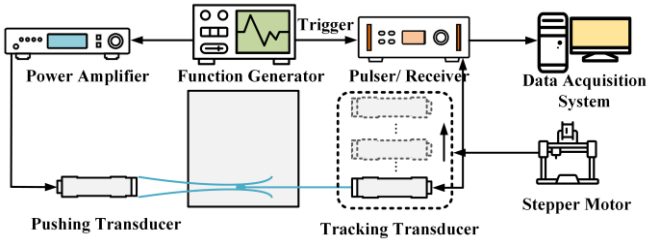

Fig. 7. Experimental system.

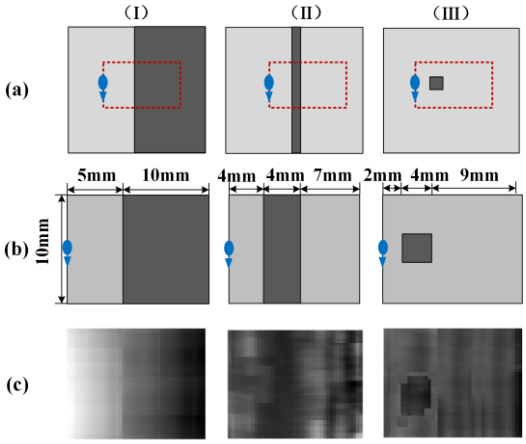

Fig. 8. Phantoms with different inclusions in experiment. (a) Experimental model. (b) Measured field. (c) Images reconstructed in logarithmic scales.

5. CONCLUSION

The relationship between the stiffness of the media and the axial-directional displacements in lateral dimension at the focal depth has been established through theoretical derivation, simulation and experimental verification. The displacement responses in lateral dimension at the focal depth have been analysed, which illustrates that the logarithm of the maximum displacement is linear with the logarithm of the lateral distance with the value of Y-intercept inversely related to the Young's modulus of the media. Therefore, a novel ARFI imaging method which detects the induced displacements at the focal point as well as in the lateral dimension at the focal depth is proposed. The simulation and experimental results have demonstrated that the elastic

distribution of the measured field can be reconstructed by the maximum displacements in lateral dimension directly, without scanning the measured field by pushing transducer.

Compared with SWEI method, the images of measured field are reconstructed by maximum displacements in the lateral dimension directly, rather than calculating the propagation velocity of shear wave by the time information of displacements at these different lateral locations. Traditional ARFI imaging method is usually used to obtain the elastic properties of media by detecting the induced displacement at the focal point. While, for this proposed method, the elastic properties of media are not only evaluated by the induced displacement at the focal point, but also by the induced displacement in lateral dimension at the focal depth. In this way, the number of excitations can be decreased, and the imaging efficiency could be further improved if the tracking transducer is a phased array. Therefore, it is expected to reduce patient acoustic exposure and transducer heating to reduce damage to soft tissues.

However, due to the attenuation of shear wave propagation, the displacements generated at different positions in the lateral direction are different. Therefore, some compensation algorithms still need to be applied to improve the attenuation of displacements in lateral direction in future.

ACKNOWLEDGMENT

The authors would like to appreciate the support from the National Natural Science Foundation of China (No. 61671322).

REFERENCES

Bercoff, J., Tanter, M., Muller, M., and Fink, M. (2004). The role of viscosity in the impulse diffraction field of elastic waves induced by the acoustic radiation force. *IEEE Trans. Ultrason., Ferroelect., Freq. Contr.,* volume (51), 1523-1536.

Dietrich, C. F., Bamber, J., Berzigotti, A., *et al.* (2017). EFSUMB Guidelines and recommendations on the clinical use of ultrasound elastography, update 2017 (long version). *Ultraschall. Med.,* volume (34), 169-184.

Doherty, J. R., Trahey, G. E., Nightingale, K. R., and Palmeri, M. L. (2013). Acoustic radiation force elasticity imaging in diagnostic ultrasound. *IEEE Trans. Ultrason., Ferroelect., Freq. Contr.,* volume (60), 685-701.

Doyley, M. M. (2012). Model-based elastography: a survey of approaches to the inverse elasticity problem. *Phys. Med. Biol.,* volume (57), R35-R73.

Doyley, M. M., and Parker, K. J. (2014). Elastography general principles and clinical applications. *Ultrasound Clin.,* volume (9), 1-11.

Hall, T. J., Bilgen, M., Insana, M. F., and Krouskop, T. A. (1997). Phantom materials for elastography. *IEEE Trans. Ultrason., Ferroelect., Freq. Contr.,* volume (44), 1355-1365.

Li, G. Y., and Cao, Y. P. (2017). Mechanics of ultrasound elastography. *Proc. R. Soc. A.,* volume (473), 20160841.

Nightingale, K. R., Palmeri, M. L., Nightingale, R. W., and Trahey, G. E. (2001). On the feasibility of remote palpation using acoustic radiation force. *J. Acoust. Soc. Am.,* volume (110), 625-634.

Qian, X. J., Ma, T., Yu, M. Y., *et al.* (2017). Multi-functional ultrasonic micro-elastography imaging system. *Sci. Rep.,* volume (7), 1230.

Rosenzweig, S., Palmeri, M., and Nightingale, K. R. (2015). Analysis of rapid multi-focal-zone ARFI imaging. *IEEE Trans. Ultrason. Ferroelectr., Freq. Control,* volume (62), 280-289.

Sarvazyan, A. P., Rudenko, O. V., Swanson, S. D., *et al.* (1998). Shear wave elasticity imaging: a new ultrasonic technology of medical diagnostics. *Ultrasound in Med. & Biol.,* volume (24), 1419-1435.

Torr, G. R. (1984). The acoustic radiation force. *Am. J. Phys.*, volume (52), 402-408.

Viola, F., and Walker, W. F. (2003). A comparison of the performance of time-delay estimators in medical ultrasound. *IEEE Trans. Ultrason. Ferroelectr., Freq. Control,* volume (50), 392-401.

Westervelt, P. J. (1951). The theory of steady forces caused by sound waves. *J. Acoust. Soc. Am.,* volume (23), 312-315.